Constraining Directional Modulation Transmitter Radiation Patterns

Ding, Y., & Fusco, V. F. (2014). Constraining Directional Modulation Transmitter Radiation Patterns. *IET Microwaves, Antennas and Propagation*, *8*(15), 1408-1415. https://doi.org/10.1049/iet-map.2014.0042

Published in:
IET Microwaves, Antennas and Propagation

Document Version:
Early version, also known as pre-print

Constraining Directional Modulation Transmitter Radiation Patterns

Yuan Ding and Vincent F. Fusco
The ECIT Institute Queens University of Belfast
Belfast, BT3 9DT, UK
v.fusco@qub.ac.uk

Abstract— **An iterative pattern synthesis approach for directional modulation (DM) transmitters is presented in this paper. Unlike all previous work this paper offers the first discussion on constraining DM transmitter far field radiation patterns so that energy is primarily concentrated in the spatial direction where low bit error rate (BER) is to be achieved, while interference projected along other directions is reduced.**

Keywords- Bit error rate, directional modulation, fast Fourier transform, pattern synthesis.

1. INTRODUCTION

Recently, directional modulation (DM) technology has been investigated as means for implementing physical-layer security in wireless communications [1–15]. DM is a transmitter technology that is able to distort transmitted signal constellation points along all selected spatial directions while leaving the constellation points along an a-priori defined direction in free space unaltered so that low bit error rate (BER) can be obtained along the specified direction. This functionality can be obtained by imposing suitable baseband signals directly onto the DM array beam-forming networks, using variable RF phase shifters and attenuators [4–9], or directly at the antenna radiators [10] in an actively driven antenna array. The DM concept was developed and mathematically rigorous necessary and sufficient condition for achieving DM properties were

formally derived in [14].

To date actively driven DM transmitter arrays, [4], [5], [8–10], are synthesized by minimizing appropriately designed cost functions which link array settings directly to BER spatial distributions without regard to far-field radiation pattern control. In some applications, e.g., where co-system location is important we require, in addition to preferred BER results, low received energy along unselected directions. This cannot be achieved by previously reported BER based DM synthesis methods.

To address this problem this paper suggests a constrained far-field pattern synthesis approach applicable for DM synthesis. The objective of this paper is to show for the first time, with minimal sacrifice on the earlier DM security properties, how the far-field patterns of DM systems can be manipulated in a pre-defined manner to adapt them to scenarios where spatial radiation masks have been imposed, e.g., in order to minimize interference. This is equivalent to seeking a subset of orthogonal vectors, [14], that meet desired far-field pattern requirements.

In Section 2 of this paper, the proposed DM iterative pattern synthesis approach is introduced. This approach developed is compatible with both static and dynamic DM systems as defined in [16]. Several exemplar synthesis results under various pattern constraints are illustrated in Section 3. Finally conclusions are drawn in Section 4.

2. PROPOSED DM CONSTRAINED PATTERN SYNTHESIS

We confine our discussion to uniformly half-wavelength spaced 1D DM transmitter arrays operating in free space. The arrangement is shown in Fig. 1 with DM properties illustrated for QPSK modulation scheme. Each antenna element is actively excited independently. Matched electromagnetic polarization between transmitters and receivers is assumed.

The proposed approach is now described;

1) For each symbol transmitted select initial array amplitude and phase excitation values for each array element.

2) Calculate far-field patterns from the array excitations. In this paper it is assumed that each array element has an ideal isotropic active element pattern (AEP) [17]. Thus far-field patterns can be easily computed via the inverse fast Fourier transform (IFFT).

3) Individually scale the magnitude patterns according to required signal to noise ratio (SNR) and shift the phase patterns to form standard constellation diagrams in IQ space along a specified communication direction. The details for constellation reshaping are described in [8].

4) Adapt the resulting far-field patterns to the templates, which are defined according to the system requirements.

5) Calculate array excitations for each unique symbol from the adapted far-field patterns via the fast Fourier transform (FFT).

6) If required, apply further DM array excitation constraints imposed by the chosen DM physical structures.

7) Repeat step 2), and adapt the resulting far-field patterns to standardize the modulation scheme constellation type along the desired communication directions as in step 3).

8) Iterate steps 4) to 7) until the far-field patterns satisfy the imposed mask templates or the maximum iteration number is reached.

9) Calibrate the excitations according to the last adaptation in step 7). This is done through scaling excitation magnitudes and shifting excitation phases by the same coefficients used in

the step 7) during the last iteration.

The above synthesis procedure is summarized using the flow chart presented in Fig. 2. The steps 1) and 4) are further discussed with examples in the next section.

3. KEY EXAMPLES

Based on the synthesis procedure described in Section 2, several key examples to illustrate how the far-field patterns and BER performance can be manipulated are now described. An 11-by-1 (N = 11) element array and QPSK modulation with Gray-coding projected along a desired low BER communication direction of 60° (boresight at 90°) are adopted hereafter. This secured communication direction can be steered by spatially shifting far-field pattern masks. The number of points for the IFFT and FFT used in the synthesis steps 2) and 5) is chosen to be 4096, and the maximum iteration number is set to 500. All results are obtained using MATLAB 2013a [18].

1. Example 1

Constraints: Far-field power spatial distribution masks only, identical for each QPSK symbol.

In a wireless point-to-point communication system, normally it is desirable that the majority of energy is radiated towards a preferred polarization matched receiver location. In [14] it was revealed that DM transmitter arrays generally radiate in an un-constrained manner energy into all spatial directions. We will now show that it is reasonable to set a spatial power mask for a DM transmitter array, e.g., as shown in Fig. 3 (a), in order to maximize transmitted power along a pre-selected low BER spatial direction while simultaneously suppressing power radiated elsewhere. The width of the rectangular mask in this example is chosen as the first null beamwidth (FNBW) of a corresponding conventional uniform tapered phased array steered to

60°, in this example 24.5°, from 47° to 71.5°. To facilitate discussions we define the spatial region where the rectangular part of the mask occupies as in-band, and attach the label of out-band to directions elsewhere. The in-band and out-band mask levels are set to be several dB higher than the main beam and sidelobes in the conventional array, allowing extra power to be introduced into the system in order to enable DM characteristics. This aspect was described in [14]. In the example here 2 dB and −10 dB respectively are used for peak main beam and average sidelobe levels. The power pattern adaption in the synthesis step 4) is applied: if the calculated far field pattern magnitudes are greater than the mask they are forced to the mask value. Otherwise, they are left unaltered.

In order to find suitable initial excitation values as described in the step 1) in the last section, we perform the following;

- Generate the excitation required to steer a conventional array to the preferred direction where low BER is required, 60° in this example.
- Randomize the magnitudes within the average power limit and phases of the excitations of 50% of the array elements. The choice of the elements undergoing in this procedure is also random.

Using this procedure the resulting set of excitations obtained generates far-field patterns with main beam approximately pointing to the selected communication direction, while preserving sufficient randomness for different QPSK symbols transmitted.

A typical set of results for a static QPSK DM system is shown in Fig. 3, with initial and final synthesized array excitations listed in Table 1. Along 60°, selected as the preference low BER direction in this example, it can be seen that the magnitudes of the four QPSK symbols overlap

each other, and that their phases are 90° spaced, indicating that a standard QPSK constellation diagram, i.e., a central symmetric square in IQ space, is formed along this direction. The constellation patterns detected in all other directions are scrambled. Importantly, and different to previous DM works [4–15], the far-field power patterns lie below the pre-defined power spatial mask, making this DM system more efficient with regard to spatial radiation energy spread, and therefore generating less interference to other systems within its radiation coverage area.

It needs to be pointed out that when compared with the corresponding conventional phased beam-steering array with the same power gain along the desired spatial direction, extra energy of P_e (unit in dB) is projected into unselected communication directions, 1.51 dB for the example DM transmitter in Table 1. This energy is exploited to enable the DM functionality, i.e., constellation distortion along undesired directions. Equivalently we can say that when compared with a conventional phased beam-steering array radiating the same total power, the power gain along the pre-specified communication direction in a DM transmitter is G_d dB lower. G_d equals P_e, see (1). Consequently hereafter we refer to the conventional array as a uniformly tapered phased beam-steering array with the same power gain as that of a DM array along its prescribed communication direction.

$$G_d = 20 \cdot \log_{10}\left(N \cdot \sqrt{\frac{10^{\left\{10 \cdot \log_{10}\left[(1/N)^2 \cdot N\right] + P_e\right\}/10}}{N}} \right) = P_e \quad \text{(dB)} \tag{1}$$

If an advanced QPSK receiver, i.e., one which enables ‘minimum Euclidean distance decoding’ [16], is used for detection then low BER can be obtained, in addition to 60°, at around 20° and 100°, as shown in Fig. 4. This is due to the fact that the phases along these two directions are reasonably spread, Fig. 3 (b). The standard QPSK receivers in Fig. 4 decode

signals based on which quadrants the received symbols locate in IQ space. All of the BERs in this paper are obtained for a random QPSK data stream with a length of 10^6 symbols under SNR of 23 dB. Throughout this paper we assume the worst case security scenario, namely, that receivers know the mappings between bits and constellation points irrespective of whether constellation diagrams are distorted or not. Details of BER calculation can be found in [16]. We set SNR to 23 dB, since at this level the first BER sidelobe in the conventional array reaches around 10^{-3}, making BER sidelobe comparison visually noticeable in a logarithmic scale. In order to return high BER values in all unselected directions, we will impose constraints on far-field phase patterns during the iteration process, this is illustrated in example 2.

2. Example 2

Constraints: the far-field power spatial distribution masks used in the example 1, and out-band far-field phase template.

In addition to the power masks used in the example 1, here we impose the phase constraint in the out-band spatial region in the synthesis step 4). The spatial phase variation of symbol '11' in the out-band is adopted as the phase template, any of the other symbols could equally have been used, a 10° phase tolerance with respect to the phase template is permitted.

Fig. 5 shows example synthesized far-field patterns for each unique QPSK symbol when both power and phase constraints are imposed. Compared with their counterparts in Fig. 3, the phase curves for each QPSK symbols are clustered together in the out-band spatial region in order to retain high out-band BER. For this example DM array, the extra power P_e is 2.45 dB, nearly 1 dB higher than that in the example 1. It can be observed in Fig. 6 that under high SNR scenario BER sidelobes in the synthesized static DM system are greatly suppressed compared with those in the conventional system. In Fig. 6 (b) constellation patterns in the both systems along the 76°

direction, which is the direction of the first sidelobe in the conventional transmitter, are also depicted. We can see that four QPSK symbols in the DM system, unlike those forming a standard square in the conventional system, are confined in a small area in the second quadrant, this results in high BER values.

In Fig. 6 (b), we find that the BER sidelobes can be effectively suppressed when the phase constraint is imposed during the iteration process. Whereas, if the static DM is constructed, the security performance in in-band region is not enhanced, i.e., the BER beamwidth for the advanced QPSK receiver case is greater than that in the conventional system. This aspect is studied in example 3.

3. Example 3

Constraints: in-band shifted far-field power spatial distribution masks, and out-band far-field phase template.

In order to narrow the in-band BER beamwidth we shift the in-band region differently for each QPSK symbol. This perturbs both magnitudes and phases around the desired communication direction. Fig. 7 presents a typical result of synthesized DM far-field patterns when the power pattern in-band masks are spatially shifted and phase constraints are imposed in their respective out-band regions. In this example, we shift the in-band regions by ± 7° for each symbol and slightly increase of the out-band level by 1 dB, as seen in Fig. 7 (a). For SNR of 23 dB Fig. 8 shows that for both receiver types the in-band BER beamwidths are narrowed with respect to the example 2. Narrower BER beamwidths are achieved at the expense of a higher P_e of 4.26 dB and increased overshooting of the power masks, see Fig. 7 (a).

4. Example 4

Constraints: far-field power spatial distribution masks with a notch, and out-band far-field phase template.

The following example is presented in order to show that we can eliminate interference to other known friendly users caused by the DM transmitter without much compromising the BER performance obtained in the earlier examples presented above. We proceed by inserting a notch around the known friendly user direction into the power mask. In the example here we insert a notch of 10° width centered at 90° with a suppression level of −15 dB into the power mask. The synthesized far-field pattern results are shown in Fig. 9. The resulting power levels for every QPSK symbols along 90° are less than −20 dB, which largely prevents signal energy from being projected towards the friendly node.

Comparing the calculated BER results of this synthesized QPSK DM system in Fig. 10 with those in Fig. 6(b), it is found that they are similar to each other except slightly narrower BER beamwidths in this example. This is a result of the 1 dB lifted out-band level. The extra power P_e of this synthesized DM array radiated compared with that of the conventional array is 2.3 dB, the same level as that in the example 2.

To enable example verification by interested readers, synthesized excitations for examples 2 to 4 are provided in Table 2.

4. CONCLUSION

A technique for controlled DM transmitter far-field pattern synthesis was proposed and discussed. Selected synthesis examples show the means for, and extent by which, key far-field radiation characteristics can be manipulated by imposing various magnitude or magnitude and

phase constraints applied during pattern iteration processes. This proposed pattern synthesis approach allows DM systems to operate in an electromagnetically green fashion which requires the spatial control of unwanted radiation in non-preferred radiation directions, a feature not previously possible with DM systems.

5. ACKNOWLEDGMENT

This work was sponsored by the Queen's University of Belfast High Frequency Research Scholarship.

6. REFERENCES

[1] Babakhani, A., Rutledge, D.B., Hajimiri, A.: 'Transmitter architectures based on near-field direct antenna modulation', *IEEE J. Solid-State Circuits*, 2008, 43, pp. 2674–2692

[2] Babakhani, A., Rutledge, D.B., Hajimiri, A.: 'Near-field direct antenna modulation', *IEEE Microw. Mag.*, 2009, 10, pp. 36–46

[3] Chang, A.H., Babakhani, A., Hajimiri, A.: 'Near-field direct antenna modulation (NFDAM) transmitter at 2.4 GHz'. Int. Symp. Antennas and Propagation Society, 2009. APSURSI'09. IEEE, pp. 1–4

[4] Daly, M.P., Bernhard, J.T.: 'Directional modulation technique for phased arrays', *IEEE Trans. Antennas Propag.*, 2009, 57, pp. 2633–2640

[5] Daly, M.P., Daly, E.L., Bernhard, J.T.: 'Demonstration of directional modulation using a phased array', *IEEE Trans. Antennas Propag.*, 2010, 58, pp. 1545–1550

[6] Shi, H.Z., Tennant, A.: 'Direction dependent antenna modulation using a two element array'. Proc. Fifth European Conf. Antennas and Propagation (EUCAP), 2011, pp. 812–815

[7] Shi, H.Z., Tennant, A.: 'An experimental two element array configured for directional antenna modulation'. Proc. 2012 Sixth European Conf. Antennas and Propagation (EUCAP), 2012, pp. 1624–1626

[8] Ding, Y., Fusco, V.: 'BER driven synthesis for directional modulation secured wireless communication', *International Journal of Microwave and Wireless Technologies*, 2014, 6, (02), pp. 139–149

[9] Ding, Y., Fusco, V.: 'Directional modulation transmitter synthesis using particle swarm optimization'. Antennas and Propagation Conference (LAPC), Loughborough, UK, Nov. 11–12 2013, pp. 500–503

[10] Daly, M.P., Bernhard, J.T.: 'Beam steering in pattern reconfigurable arrays using directional modulation', *IEEE Trans. Antennas Propag.*, 2010, 58, pp. 2259–2265

[11] Valliappan, N., Lozano, A., Heath, R.W.: 'Antenna subset modulation for secure millimeter-wave wireless communication', *IEEE Trans. Commun.*, 2013, 61, pp. 3231–3245

[12] Zhang, Y., Ding, Y., Fusco, V.: 'Sidelobe modulation scambling transmitter using Fourier Rotman lens', *IEEE Trans. Antennas Propagat.*, 2013, 61, pp. 3900–3904

[13] Ding, Y., Fusco, V.: 'Sidelobe manipulation using Butler matrix for 60 GHz physical layer secure wireless communication'. Antennas and Propagation Conference (LAPC), Loughborough, UK, Nov. 11–12 2013, pp. 61–65

[14] Ding, Y., Fusco, V.: 'A vector approach for the analysis and synthesis of directional modulation transmitters', *IEEE Trans. Antennas Propagat.* 2014, 62, pp. 361–370

[15] Ding, Y., Fusco, V.: 'Vector representation of directional modulation transmitters'. Proc. 2014 8th European Conf. Antennas and Propagation (EUCAP), Hague, Netherlands, 2014, pp. 332–336

[16] Ding, Y., Fusco, V.: 'Establishing metrics for assessing the performance of directional modulation systems', *IEEE Trans. Antennas Propagat.*, 2014, 62, (5), pp. 2745–2755

[17] Pozar, D.M.: 'The active element pattern', *IEEE Trans. Antennas Propagat.*, 1994, 42, pp. 1176–1178

[18] MATLAB Release: The MathWorks, Inc., Natick, MA, USA, 2013

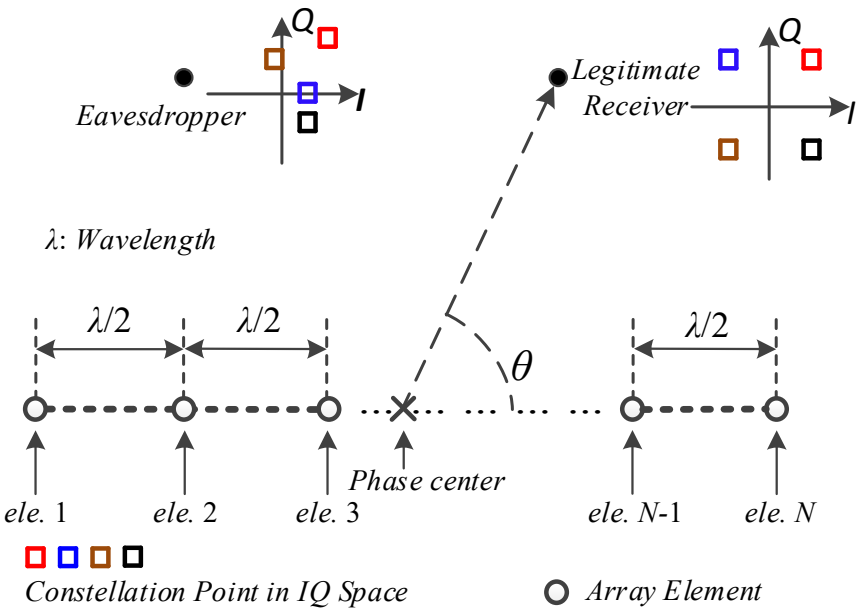

Figure 1. The arrangement of a uniformaly half-wavelength spaced 1D DM transmitter array operating in free space. The DM property, i.e., standard constellation patterns are preserved along desired communication direction, is illustrated for QPSK modulation scheme.

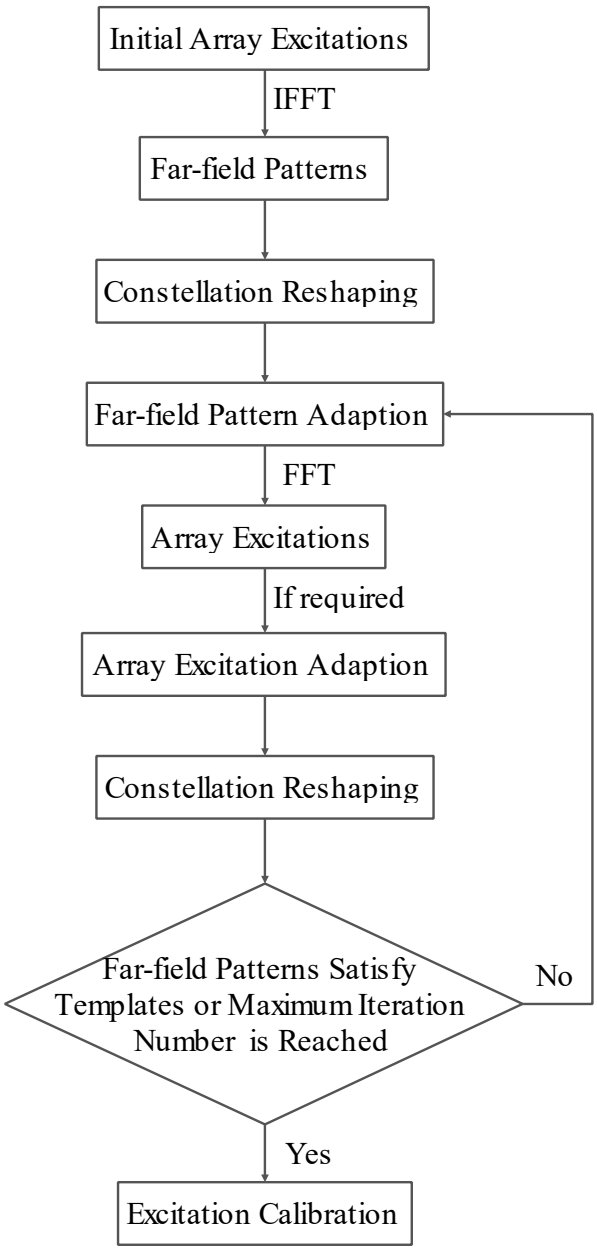

Figure 2. Flow chart for proposed DM far-field pattern synthesis procedure.

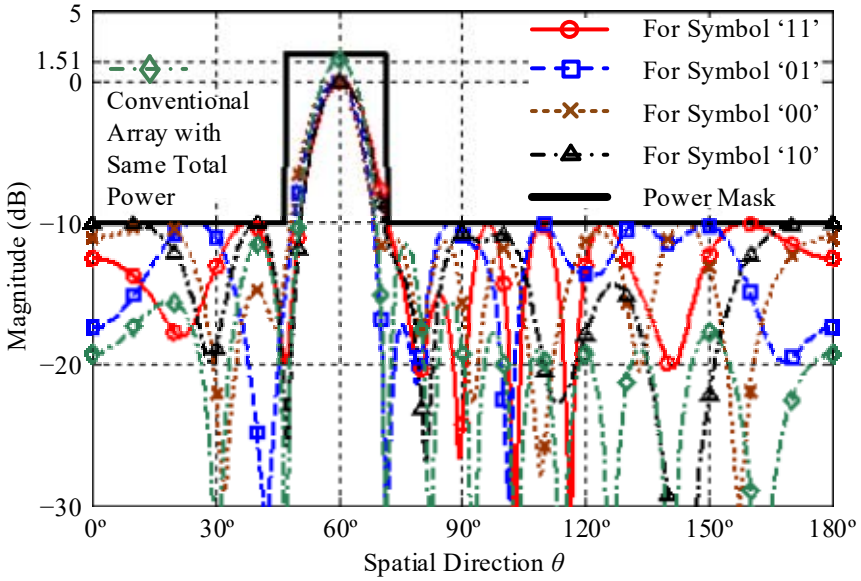

(a)

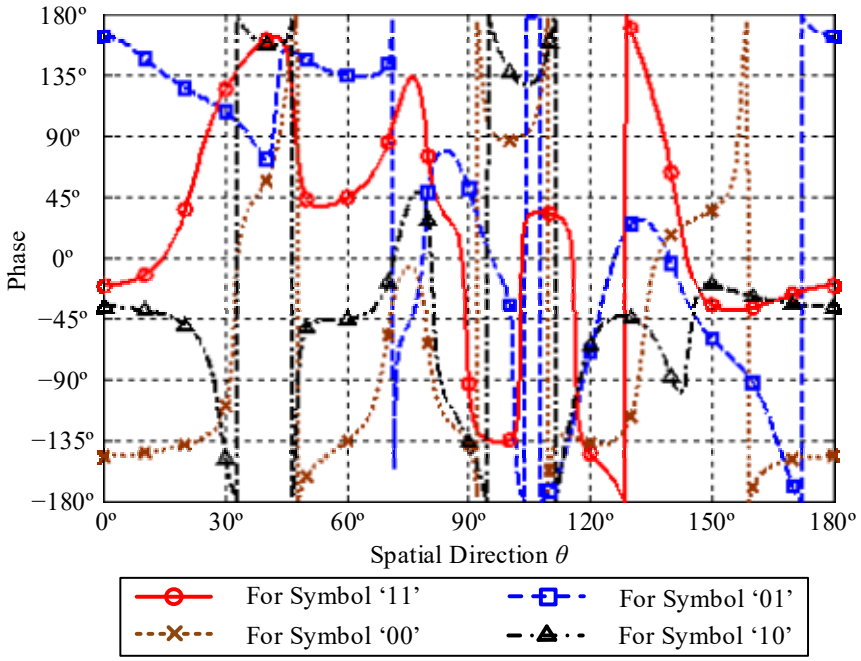

(b)

Figure 3. Typical synthesized far-field (a) power patterns and (b) phase patterns for each QPSK symbol. The power mask is also depicted in (a).

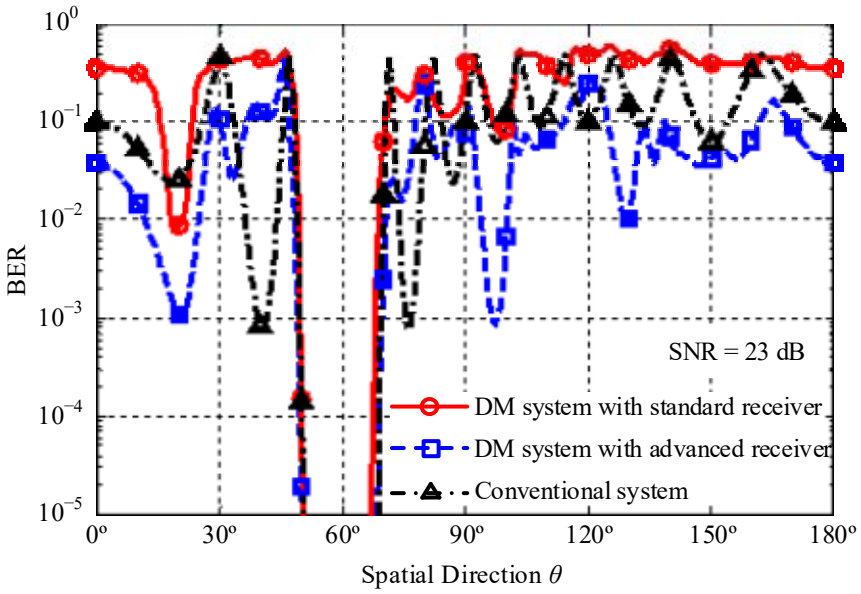

Figure 4. BER spatial distributions for the synthesized static DM system in Fig. 3.

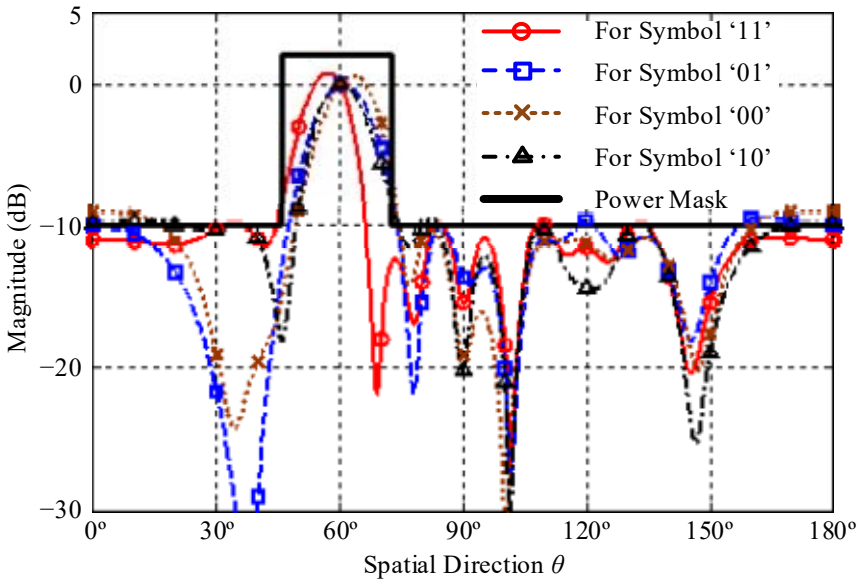

(a)

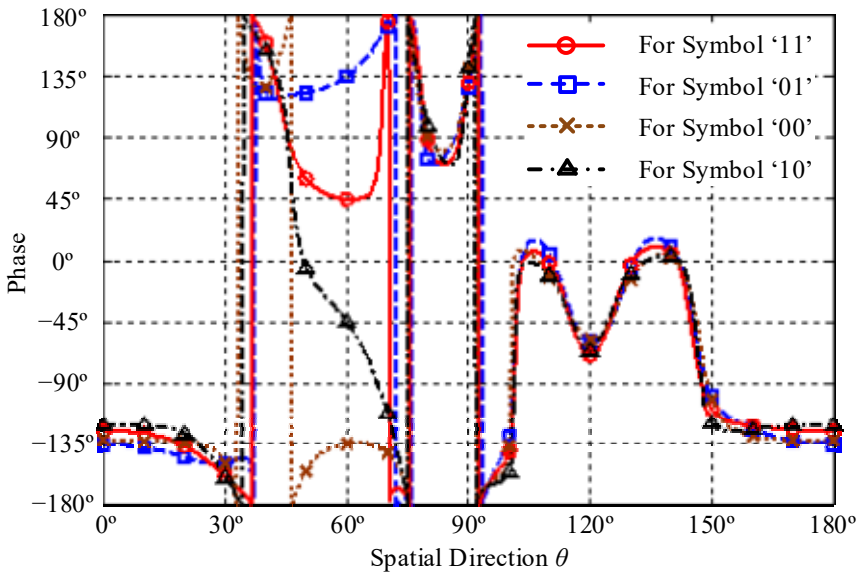

(b)

Figure 5. Typical synthesized far-field (a) power patterns and (b) phase patterns for each QPSK symbol. The power mask is shown in (a). The phase constraint is set in the out-band region using the spatial phase varaition of symbol '11' as the reference template.

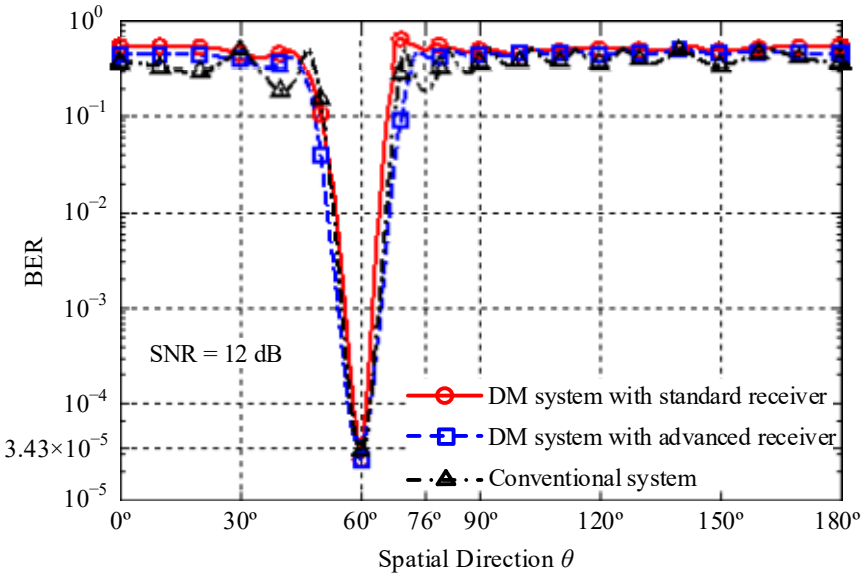

(a)

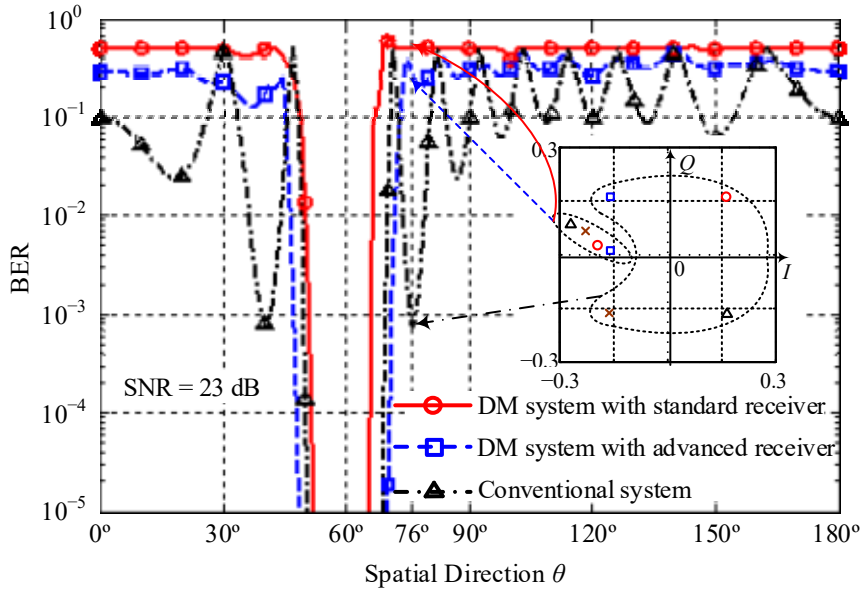

(b)

Figure 6. BER spatial distributions for the synthesized static DM system in Fig. 5 and the conventional system for SNRs of (a) 12 dB and (b) 23 dB. The constellation patterns along 76° in the both systems are also depicted in (b).

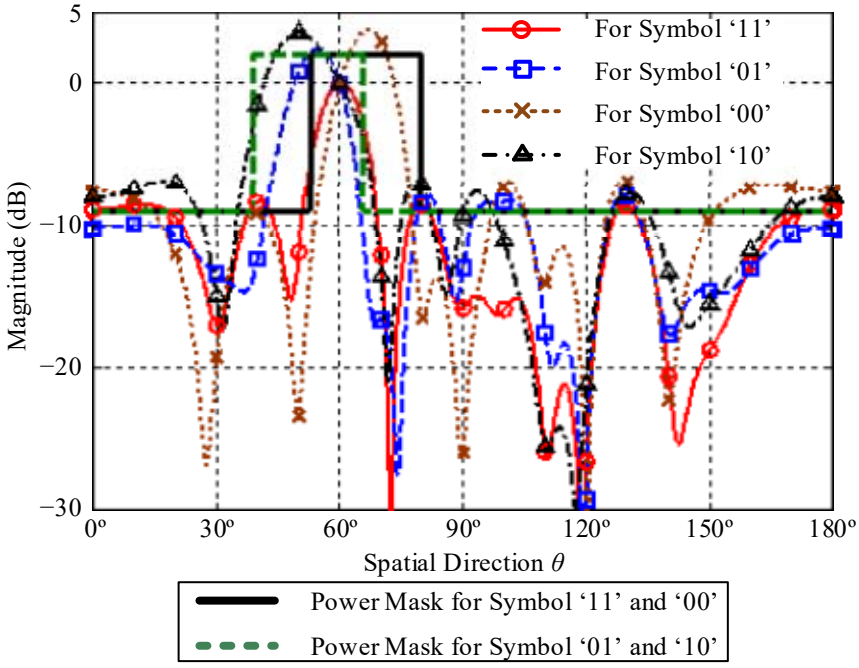

(a)

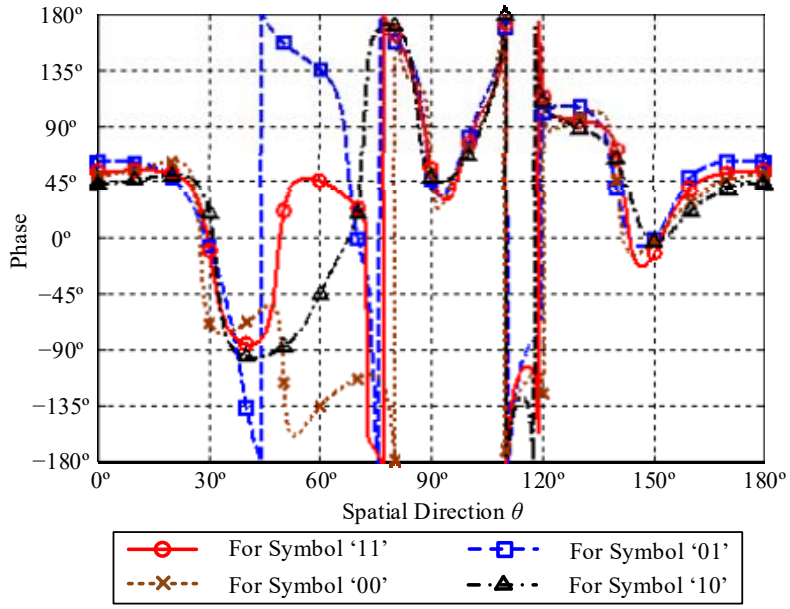

(b)

Figure 7. One typical synthesized far-field (a) power patterns and (b) phase patterns for each QPSK symbol. The power masks for different QPSK symbols are also shown in (a). The phase constraint is set in the out-band regions with the phases for symbol '11' as the reference template.

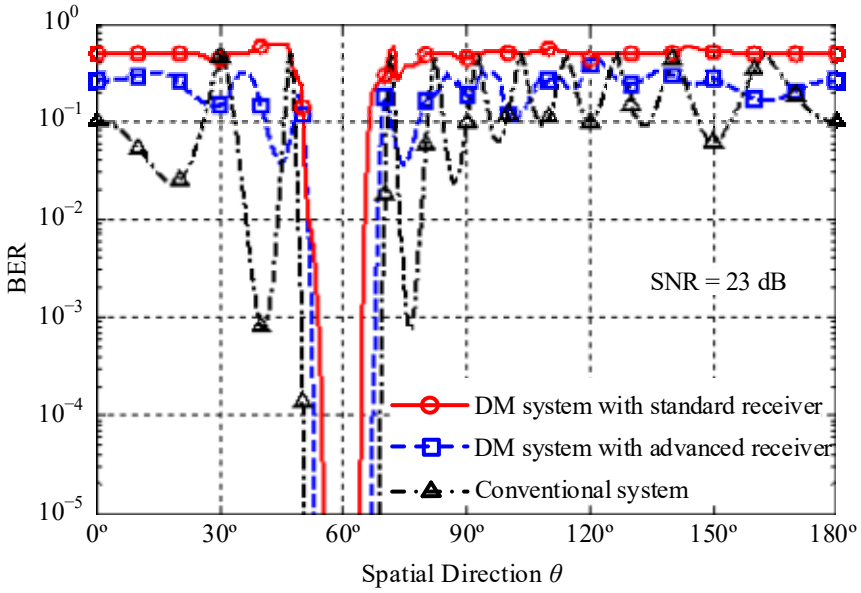

Figure 8. BER spatial distributions for the synthesized static DM system in Fig. 7 and the conventional system.

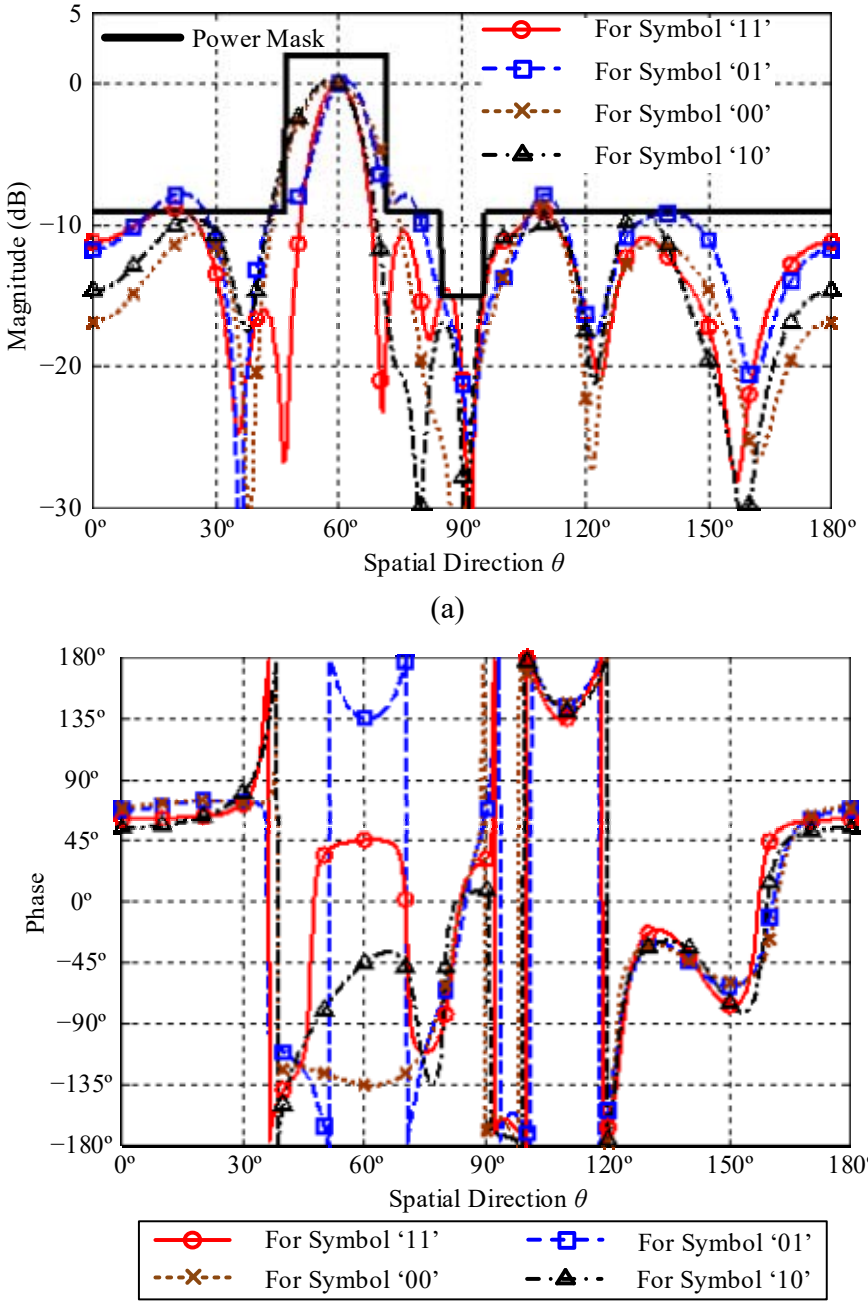

Figure 9. Typical synthesized far-field (a) power patterns and (b) phase patterns for each QPSK symbol. The power mask with a notch along boresight is also shown in (a). The phase constraint is set in the out-band region with the phases for symbol '11' as the reference template.

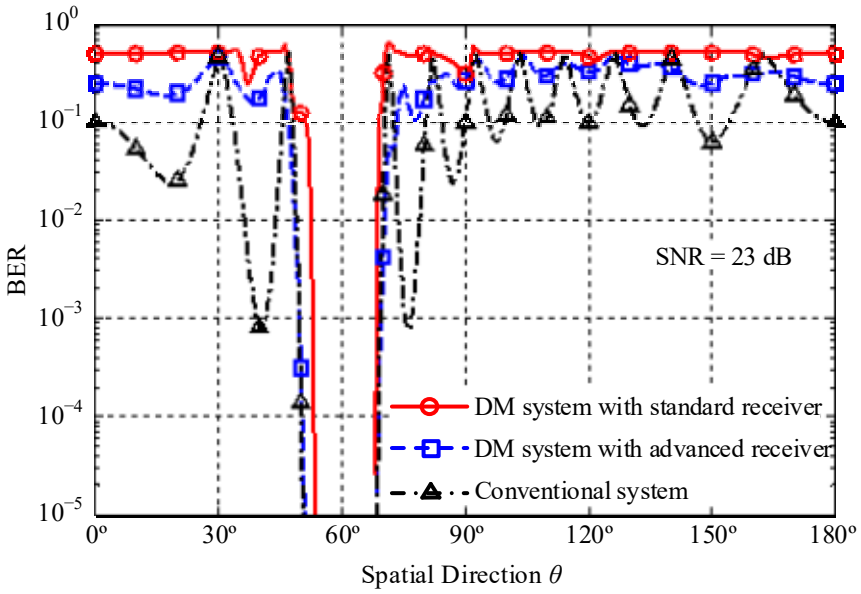

Figure 10. BER spatial distributions for the synthesized static DM system in Fig. 9 and the conventional system.

Table 1. The initial and final synthesized array excitations for the static QPSK DM array in Fig. 3.

		Symbol '11'		Symbol '01'		Symbol '00'		Symbol '10'	
Array Excitations		Magnitude ($\times 10^{-1}$)	Phase (Degree)	Magnitude ($\times 10^{-1}$)	Phase (Degree)	Magnitude ($\times 10^{-1}$)	Phase (Degree)	Magnitude ($\times 10^{-1}$)	Phase (Degree)
Element 1	Initial	0.753	−39	0.909	90	0.909	90	0.909	90
	Final	1.195	126	1.016	−146	1.112	−20	0.264	61
Element 2	Initial	0.823	88	0.909	0	0.909	0	0.114	82
	Final	1.097	47	0.247	149	1.624	−134	1.222	−55
Element 3	Initial	0.909	−90	0.851	103	0.460	58	0.909	−90
	Final	1.183	−100	1.214	42	0.456	128	1.077	−142
Element 4	Initial	0.909	180	0.909	180	0.909	180	0.821	95
	Final	0.997	−121	1.056	21	1.693	51	1.415	116
Element 5	Initial	0.909	90	0.628	137	0.909	90	0.909	90
	Final	1.338	149	1.314	−138	0.987	−35	1.053	74
Element 6	Initial	0.824	92	0.433	−149	0.103	19	0.208	−63
	Final	1.202	61	1.061	118	1.345	−131	1.241	−56
Element 7	Initial	0.909	−90	0.840	170	0.909	−90	0.358	28
	Final	1.186	−31	1.511	44	0.845	140	1.137	−147
Element 8	Initial	0.351	−57	0.477	71	0.909	−180	0.909	−180
	Final	0.985	−105	1.243	−54	0.403	38	1.159	−171
Element 9	Initial	0.909	90	0.909	90	0.424	−170	0.763	−69
	Final	1.012	142	0.352	−9	0.346	−143	0.366	106
Element 10	Initial	0.746	50	0.909	0	0.863	−24	0.909	0
	Final	0.922	−56	1.145	130	1.343	−147	1.183	−58
Element 11	Initial	0.658	−64	0.909	−90	0.776	169	0.909	−90
	Final	0.823	−29	1.173	28	0.494	101	0.921	−155

Table 2. The final synthesized array excitations for the static QPSK DM arrays in the examples 2 to 4.

		Symbol '11'		Symbol '01'		Symbol '00'		Symbol '10'	
	Array Excitations	Magnitude ($\times 10^{-1}$)	Phase (Degree)	Magnitude ($\times 10^{-1}$)	Phase (Degree)	Magnitude ($\times 10^{-1}$)	Phase (Degree)	Magnitude ($\times 10^{-1}$)	Phase (Degree)
Example 2	Element 1	1.097	139	0.846	160	0.117	104	0.711	105
	Element 2	0.746	109	1.121	149	1.126	−156	0.279	−137
	Element 3	0.854	5	1.573	55	1.252	106	0.313	−176
	Element 4	1.326	−152	0.755	−68	0.924	67	1.443	145
	Element 5	1.271	167	1.801	−136	1.445	−69	0.589	28
	Element 6	0.989	46	1.103	145	1.566	−128	1.284	−62
	Element 7	1.356	12	2.319	62	2.157	104	0.623	145
	Element 8	1.705	−153	0.530	−69	1.047	78	1.629	149
	Element 9	1.436	97	0.287	−119	1.092	−3	1.897	50
	Element 10	1.012	−31	0.467	−141	1.157	−102	1.715	−56
	Element 11	1.060	−71	0.752	−14	0.347	−76	1.087	−105
Example 3	Element 1	0.647	−141	1.282	−76	2.167	−109	0.391	112
	Element 2	1.129	25	0.556	−77	0.636	155	2.393	−6
	Element 3	1.088	−56	0.614	87	1.266	79	2.151	−102
	Element 4	1.118	−143	1.356	4	2.166	26	2.056	142
	Element 5	1.107	127	1.071	−109	1.882	−43	2.182	37
	Element 6	1.626	55	2.163	121	1.177	−126	1.269	−37
	Element 7	0.645	−112	1.325	77	2.835	169	2.559	172
	Element 8	0.166	−114	1.477	−37	1.829	71	2.034	53
	Element 9	1.245	130	1.645	172	1.013	61	0.249	32
	Element 10	1.239	65	1.614	92	0.321	−44	0.875	117
	Element 11	1.207	−35	1.451	−17	0.766	−75	0.857	−10
Example 4	Element 1	1.113	141	1.185	162	0.304	172	1.041	101
	Element 2	1.007	52	1.067	91	0.627	127	0.984	−20
	Element 3	1.304	−44	1.039	2	0.501	153	1.463	−111
	Element 4	0.216	35	1.849	9	2.308	47	1.904	100
	Element 5	1.330	142	1.356	−139	1.123	−49	1.202	59
	Element 6	0.964	49	1.183	167	1.771	−134	1.235	-60
	Element 7	1.037	−87	0.900	94	1.943	153	1.668	−155
	Element 8	1.500	−134	1.235	−60	0.622	42	0.797	157
	Element 9	0.162	127	1.282	−88	1.602	−44	1.191	−15
	Element 10	1.103	52	1.227	120	0.464	170	0.274	1
	Element 11	0.992	−44	0.795	7	0.273	25	0.424	−72